

Tailored Optoelectronic Materials: DES-Modified MWCNTs in PVA Matrix for Advanced Polymeric Films

Lokesh Kumar S ¹, Laveena M Vegais ¹, Sunitha Villayilveed Ramachandran Nair ², Sumaiya Tabassum ³, Mothi Krishna Mohan ², Santhosh Govindaraju ^{2,*}

¹ Department of Chemistry, CHRIST University, Bengaluru, 560029, India

² Department of Sciences and Humanities, CHRIST University, Bengaluru, 560074, India

³ Department of Chemistry, Surana College, Bengaluru, 560074, India

* Correspondence: santhosh87org@gmail.com;

Scopus Author ID 56509312200

Received: 14.6.2024; Accepted: 5.09.2024; Published: 15.04.2025

Abstract: Integrating optoelectronic functionalities with advanced materials offers exciting potential for novel composite systems. This study investigates the synthesis, characterization, and optoelectronic applications of polyvinyl alcohol (PVA) films incorporating multi-walled carbon nanotubes (MWCNTs) surface-modified with choline chloride-urea (1:2) deep eutectic solvents (DES), known as Reline. Dispersion of Reline-enhanced MWCNT within the PVA matrix is meticulously described. DES-grafted MWCNTs demonstrate improved solubility, leading to superior dispersion within the polymer, confirmed by scanning electron microscopy (SEM), Fourier-transform infrared spectroscopy (FTIR), and X-ray diffraction (XRD). The influence of Reline-grafted MWCNT loading on the films' optoelectronic properties, including optical absorbance, bandgap, and electrical conductivity, is systematically analyzed. Results show that DES-grafted MWCNTs significantly enhance these properties, indicating strong potential for these composites in optoelectronic devices such as solar cells, photovoltaics, photodetectors, and light-emitting devices.

Keywords: deep eutectic solvents; MWCNT; PVA; optoelectronics; films.

© 2025 by the authors. This article is an open-access article distributed under the terms and conditions of the Creative Commons Attribution (CC BY) license (<https://creativecommons.org/licenses/by/4.0/>).

1. Introduction

In recent years, the quest for efficient and environmentally sustainable materials has incited noteworthy advancements across diverse scientific domains, remarkably in the arena of optoelectronic devices. The unique and easily adaptable properties of polymers and polymer composites have played a pivotal role in this progress [1], making them reliable candidates for various applications [2], including integrated optics [3], optical sensors [4], microlasers [5], nanophotonics [5], optical communication [6], and data processing. The most prominent water-soluble polymer used for diverse optoelectronic devices and applications that is environmentally amicable and cost-effective is polyvinyl alcohol (PVA), one of the most essential polymers used in the industry. It ranks among the industry's most crucial polymers. PVA boasts exceptional optical characteristics and is a semicrystalline polymer with robust dielectric strength, high transparency, outstanding physical properties, and excellent film-forming ability. Since PVA is an insulator, converting this polymer to a semiconductor or conductor is challenging. An up-and-coming innovation revolves around the amalgamation of Reline, a deep eutectic solvent (DES) comprising choline chloride and urea(1:2) [7], tethered to multi-walled carbon nanotubes (MWCNTs) [8], which are subsequently dispersed within a

matrix of polyvinyl alcohol (PVA) [9]. This intricate composite material engenders many possibilities for augmenting optoelectronic device applications. Through the judicious fusion of the distinctive attributes of each constituent element, researchers have adeptly engineered thin films that exhibit remarkable characteristics [10], thereby setting the stage for captivating developments in photonics [11], electronics [11], and related disciplines [12].

This novel composite material orchestrates the synergy of several pivotal components to harness their individual merits harmoniously [12]. Reline, formed from choline chloride and urea, is celebrated for its marked attributes, including low toxicity [13], biodegradability, and exceptional solvent properties [14], rendering it a compelling contender for an array of applications [12,15]. In contrast, due to their nanoscale architecture, MWCNTs boast superlative electrical [16], thermal [17], and mechanical characteristics [14,18], thus proffering prospects for such as solar cell [19], photo voltaic, photodetectors, and light-emitting devices [16,20].

The amalgamation of this Reline-MWCNT complex within a PVA matrix begets a versatile and durable substrate for crafting thin films. PVA, a water-soluble synthetic polymer [21], is renowned for its aptitude in forming films [22], biocompatibility [23], and optical transparency [24]. By dispersing the Reline-MWCNT complex within the PVA matrix, researchers have triumphed in concocting thin films that manifest an amalgam of extraordinary properties, encompassing mechanical flexibility [25], electrical conductivity [26], and modifiable optical attributes [27].

These thin films harbor substantial potential in the realm of optoelectronic device applications [28]. Their unique amalgamation of attributes renders them amenable to an array of functionalities, such as transparent conductive layers [29], photovoltaic materials [30], and sensors [31]. Furthermore, their fabrication process affords the latitude for customized film thickness [32–34], composition, and morphology adjustments, thereby empowering researchers to tailor the material to specific device requisites.

In this context, the present investigation embarks upon an exhaustive characterization of these pioneering thin films [35]. Various analytical methodologies, including scanning electron microscopy (SEM), X-ray diffraction (XRD), UV-Vis spectroscopy, and electrical conductivity measurements, have been harnessed to comprehensively explicate the films' structural, optical, and electrical properties. These discernments furnish invaluable insights to optimize the material's performance and tailor it meticulously to the exigencies of particular optoelectronic applications.

2. Materials and Methods

2.1. Preparation of reline.

The two solid ingredients, choline chloride and urea, were thoroughly mixed to guarantee homogeneity using a stirring mechanism that rotated at 250 rpm. Under carefully controlled circumstances, a temperature of 80°C was maintained throughout the 20-minute mixing process. It is significant to note that, throughout this carefully regulated heating and stirring procedure, choline chloride and urea experienced a metamorphosis, reaching a eutectic stage where they displayed distinct liquid-like properties, indicative of the development of the deep eutectic solvent known as Reline.

2.2. Preparation of Reline grafted MWCNT.

All chemicals were purchased from Merck grade and were used as received without further purification except drying for 24 h at 50°C under vacuum to reduce the moisture content. MWCNT was functionalized by grafting the freshly prepared reline onto the surface. The preparation method entailed the incorporation of 0.1 mL of reline per 0.05 g of MWCNTs, followed by an intensive grinding procedure lasting one hour. This grinding step aimed to achieve a homogeneous and well-dispersed reline-MWCNT composite.

2.3. Preparation of polymeric films.

Reline grafted MWCNT was employed as a dispersed phase and dispersed within a 5% PVA matrix by sonicating for four hours. This sonication process was instrumental in ensuring the thorough integration of the Reline-MWCNT composite into the PVA matrix, thereby facilitating the uniform distribution of the composite within the polymer matrix. The resulting highly dispersed PVA matrix was then skillfully coated onto pristine glass substrates using a spin coater. This procedure guaranteed the deposition of a thin and uniform film of the PVA matrix, encapsulating the reline-MWCNT composite onto the glass surface. The execution of this multi-step fabrication process played a pivotal role in achieving the desired film structure and composition, which is critical for subsequent analyses and characterization.

Table 1. Composition of Reline grafted MWCNT – PVA solid polymer (SP) films.

Sl No	5%PVA solution (mL)	Reline grafted MWCNT(g)
1	1.5	0.001
2	1.5	0.002
3	1.5	0.003
4	1.5	0.004
5	1.5	0.005
6	1.5	0.006
7	1.5	0.007
8	1.5	0.008
9	1.5	0.009
10	1.5	0.01

2.4. UV-Vis spectroscopy.

The UV/Visible spectrum analysis was conducted utilizing the Ocean Optics Chem USB4 UV/Visible Spectrophotometer, a sophisticated instrument renowned for its precise spectroscopic capabilities in the UV and visible spectral domains. This versatile tool facilitated the acquisition of UV/Visible spectra, which were subjected to rigorous analysis for various optical and conductivity investigations. Notably, a set of ten distinct films, with pure polyvinyl alcohol (PVA) as the reference material, were meticulously recorded with high-resolution spectrophotometric data collection within the 200 to 800 nm range.

2.5. Fourier transform infrared spectroscopy.

The infrared spectra of all the films were meticulously analyzed utilizing a Fourier transform infrared (FTIR) Spectrometer of the Shimadzu IR Spirit-L model. The spectra acquisition was performed in the attenuated total reflectance (ATR) mode, affording the capacity to gauge the absorption of infrared radiation by the samples under scrutiny. The

spectral region examined spanned from 400 to 4000 cm^{-1} , featuring a spectral resolution of 4 cm^{-1} . The dataset was meticulously generated by accumulating a total of 40 scans, a rigorous approach chosen to ensure the attainment of a lucid and precise representation of the spectral attributes inherent to the specimens under investigation.

2.6. X-ray diffraction analysis.

X-ray diffraction (XRD) analysis of all film samples was performed using the XRDynamic 500, a state-of-the-art X-ray diffractometer manufactured by Anton Paar, renowned for its exceptional capabilities in elucidating structure modification and material properties. This sophisticated instrument facilitated the acquisition of XRD patterns, which were subsequently subjected to an in-depth examination as part of a comprehensive study.

2.7. Scanning electron microscopy.

Scanning electron microscopy (SEM) analysis of the film samples was undertaken using a cutting-edge SEM instrument to probe their morphological and microstructural characteristics. The SEM instrument employed for this study, renowned for its advanced imaging capabilities, enabled the meticulous examination of surface topography and microstructure at high magnification and resolution. All ten distinct film specimens were subjected to SEM analysis to unveil their intricate surface features and structural attributes.

2.8. Impedance spectroscopy.

Electrochemical measurements were conducted using a CH Instruments 608D analyzer. One electrode terminal was linked to the sensing probe on the electrochemical workstation, while the other terminal was connected to both the reference and counter probes on the same electrochemical workstation. The frequency under examination was configured within 1 Hz to 1 MHz, utilizing a 0.5V AC voltage in the impedance measurement program. Electrochemical impedance spectroscopy (EIS) measurements were acquired through a series of three consecutive recordings, with subsequent utilization of the average value obtained. Following each measurement cycle, the sensor rinsed using phosphate-buffered saline (PBS). It is important to note that all electrochemical measurements were conducted under ambient room temperature conditions, specifically within the range of 25 to 27°C.

3. Results and Discussion

3.1. Fourier transform infrared spectroscopy.

The spectral results of all the polymeric films are represented in Figure 1. Several prominent absorption bands were observed in the FTIR spectrum of pure PVA film, such as the strong peak at 3274 cm^{-1} corresponding to the O-H stretching vibration, indicating the presence of hydroxyl (OH) groups in the PVA polymer. The band at 2910 cm^{-1} is attributed to C-H stretching vibrations of aliphatic groups, indicating the presence of -CH₂- and -CH₃ groups in the PVA backbone. The peak at 1426 cm^{-1} is associated with C-H bending vibrations, further confirming the presence of aliphatic hydrocarbon groups. Finally, the band at 1068 cm^{-1} corresponds to C-O stretching vibrations, indicating the presence of ether groups (C-O-C) in the PVA structure. These characteristic vibrational modes indicate the molecular structure of

PVA, which contains hydroxyl and aliphatic groups, and provide valuable information for its identification and characterization.

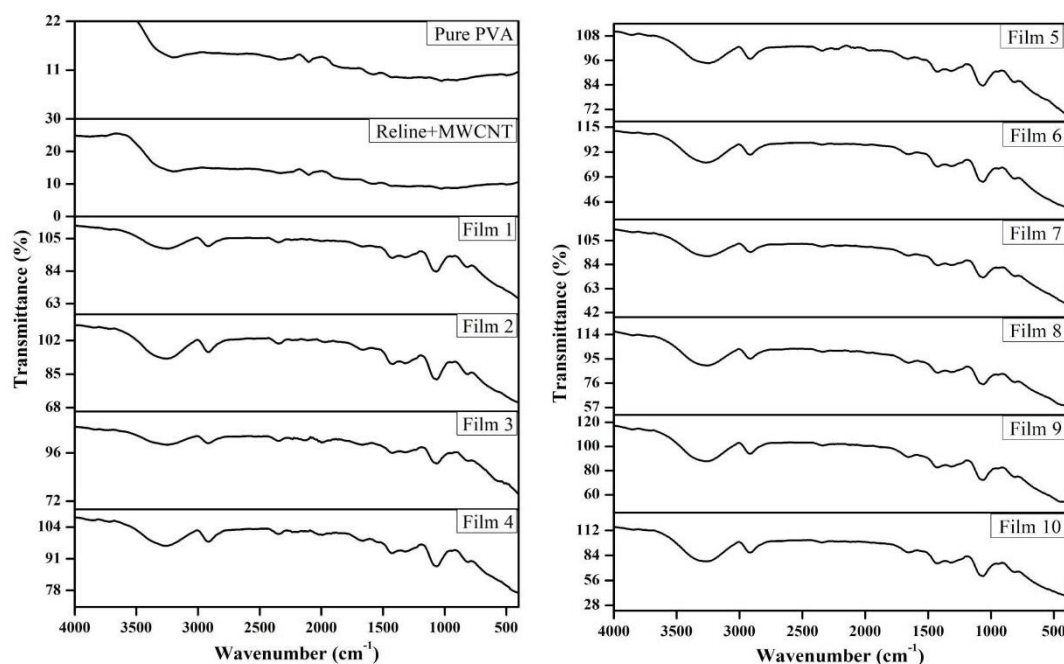


Figure 1. FTIR spectrum of all polymeric films.

The FTIR spectrum of the reline grafted MWCNT polymeric film showed a broad peak of 3250 to 3300 cm^{-1} corresponding to O-H stretching vibrations, indicative of hydroxyl groups and possibly hydrogen bonding interactions in both PVA and Reline. The bands at 2900 to 2950 cm^{-1} are associated with C-H stretching vibrations, suggesting the presence of aliphatic hydrocarbon groups in PVA and, potentially, in MWCNTs. The range of 2300 to 2350 cm^{-1} typically corresponds to the stretching vibrations of carbon-carbon interactions, which is attributed to the interaction of the Reline with the MMWCNT surfaces. The peaks at 1400 to 1450 cm^{-1} , 1300 to 1350 cm^{-1} and 1050 to 1100 cm^{-1} are likely related to C-H bending vibrations, C-O stretching, or C-O-H bending vibrations, reflecting the PVA matrix's presence. Finally, the band at 800 to 850 cm^{-1} could be attributed to vibrations associated with the MWCNTs, possibly involving structural or electronic interactions. These spectral features collectively suggest a complex interplay of functional groups, structural modifications, and interactions within the composite film.

3.2. Morphological studies.

The SEM imaging studies provided a lucid depiction of the surface morphology of the films, revealing a distinctive grainy texture characterized by micro-level roughness. This surface texture is a direct consequence of the film composition, which includes the incorporation of reline-grafted MWCNTs within a PVA matrix. The observed graininess and micro-level roughness can be attributed to the presence of MWCNTs, which introduce irregularities and microstructural features on the film's surface due to their inherent nanoscale nature. These nano-sized entities contribute to surface roughness and facilitate the creation of grain-like structures.

The acquired SEM images further revealed a compelling observation – a conspicuous and uniform dispersion of the reline-grafted MWCNTs polymeric films. This noteworthy

phenomenon is succinctly illustrated in Figure 2. The images provided unambiguous evidence of successfully integrating the reline-grafted MWCNTs into the PVA matrix, showcasing a homogenous distribution throughout the film structure.

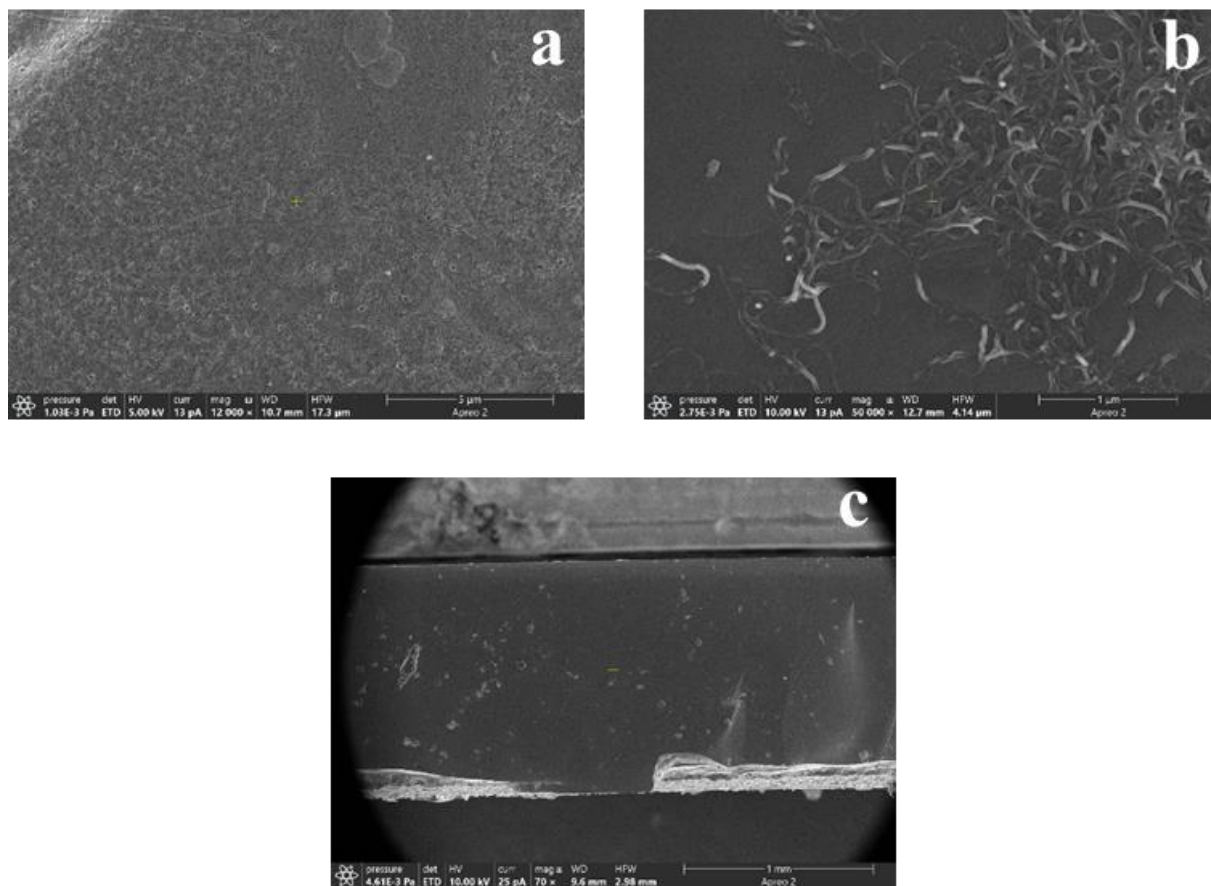


Figure 2. SEM images of film 8 (a), (b)- Lateral view of film, (c) – cross-sectional view).

The cross-sectional imaging procedure undertaken in this study proved to be exceptionally informative, providing crucial insights into the film's thickness and structural characteristics under investigation. The thickness of the film was precisely quantified and determined to be 1.18 mm through this method. This provides a precise and quantitative representation of the film's dimensional attributes. The observed thickness is a fundamental parameter in material characterization, influencing the film's mechanical, thermal, and optical properties.

3.3. X-ray diffraction analysis.

The X-ray diffraction (XRD) pattern of the films studied provides valuable insights into the structural changes induced by incorporating Reline-grafted MWCNT into the PVA solution. Figure 3 shows a noteworthy observation of the slight broadening of the XRD peak with an increase in the concentration of Reline-grafted MWCNT in the polymer matrix, which signifies a disruption in the crystalline lattice of the composite material. This broadening occurs due to the introduction of disorder as MWCNTs interfere with the regular arrangement of polymer chains. Conversely, sharp peaks are evident in the XRD pattern of pure PVA films, indicating a more ordered and crystalline structure in the absence of MWCNTs. These findings collectively support the conclusion that the inclusion of Reline-grafted MWCNTs leads to an amorphous nature in the composite material. At the same time, the purity of PVA films results

in a more organized structure, shedding light on the material's structural transformations with varying MWCNT concentrations, which is crucial for its potential applications in optoelectronic devices.

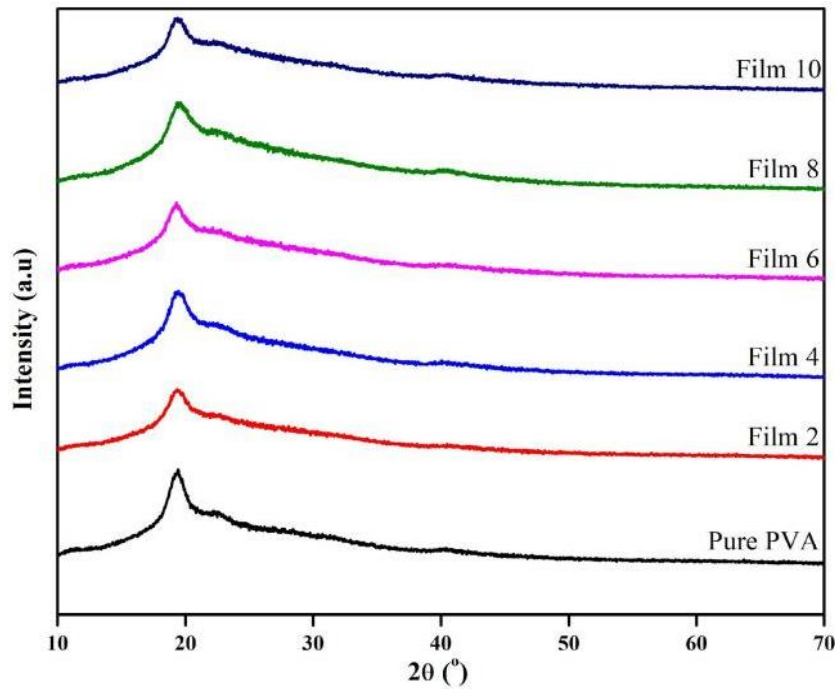


Figure 3. XRD of polymeric films.

3.4. Band gap studies.

The band gap of all the fabricated polymeric films was assessed through the Tauc plot method. This method is a widely used to estimate the band gap energy (E_g) from UV-Vis absorption data. It involves plotting the absorption coefficient (α) as a function of the photon energy ($h\nu$), where α is obtained from the absorbance (A) using equation 1, with d being the thickness of the sample and λ being the wavelength.

With the absorption coefficient data, the band gap was calculated by plotting $(\alpha h\nu)^2$ against $h\nu$ on a graph. Extrapolating the linear portion of the plot to the x-axis ($h\nu = 0$) will give the value of the band gap energy.

$$\alpha = \frac{2.303}{d} \left(\frac{A}{\lambda} \right) \quad (1)$$

The investigation into the band gap energy of PVA films modified with DES-grafted MWCNTs revealed a compelling trend (Figure 4). As the concentration of DES-grafted MWCNTs increased from Film 1 to Film 8 as the MWCNT concentration increases from Films 1 to 8, the plots reveal a systematic shift in the linear portion of the $(\alpha h\nu)^2$ vs $h\nu$ curves towards higher photon energies. This shift corresponds to a reduction in the band gap energy, evident by the leftward movement of the x-axis intercept where the extrapolated linear portion meets the horizontal axis. This phenomenon suggests an enhancement in the film's potential for light absorption and improved electronic properties. Film 8 emerged as the most promising candidate, exhibiting the lowest band gap energy among the films studied. The observed reduction in band gap energy in PVA films modified with DES-grafted MWCNTs can be attributed to several interconnected factors. Introducing MWCNTs raises a quantum confinement effect, where the nanoscale dimensions of the tubes cause energy levels to become discrete by lowering the band gap.

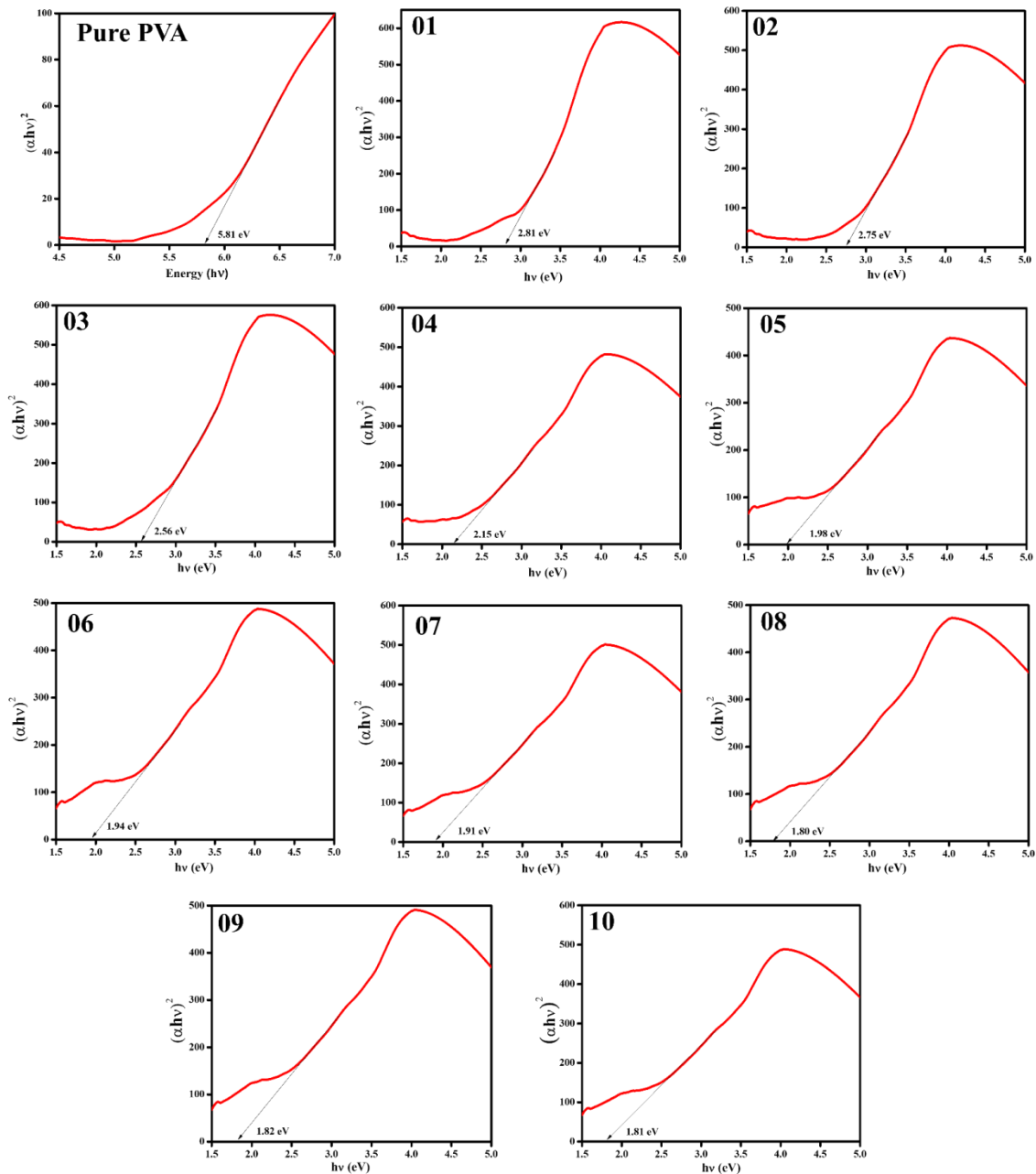


Figure 4. Band gap study of the polymeric films.

Furthermore, the high electron mobility and charge transfer capabilities of MWCNT facilitate efficient charge transport and interaction with the DES, thus promoting electron mobility and reducing the band gap. Similarly, the heightened light absorption capabilities of MWCNTs contribute to increased photon absorption, leading to more electrons being excited from the valence band to the conduction band. Surprisingly, films 9 and 10, with higher DES-grafted MWCNT concentrations, did not display a significant further reduction in band gap energy, suggesting a saturation effect. These findings underscore the importance of optimizing the composition of PVA films for tailored optoelectronic properties. Film 8 represents an ideal balance between MWCNT concentration and band gap energy reduction, making it a prime candidate for further investigation and potential applications in optoelectronic devices.

3.5. Electrical conductivity studies.

The impedance study of polymeric films (Figure 5) revealed interesting trends in electrical conductivity. Films 1 to 5 initially exhibited significantly high bulk resistivity values, <https://biointerfaceresearch.com/>

indicating poor electrical conductivity. However, a noticeable decrease in bulk resistance was observed with the subsequent films, 6 and 7, which displayed resistances of $7.2 \times 10^7 \Omega$ and $1.0 \times 10^7 \Omega$, respectively. This trend suggests that the conductivity improved as the concentration of Reline-grafted MWCNTs increased.

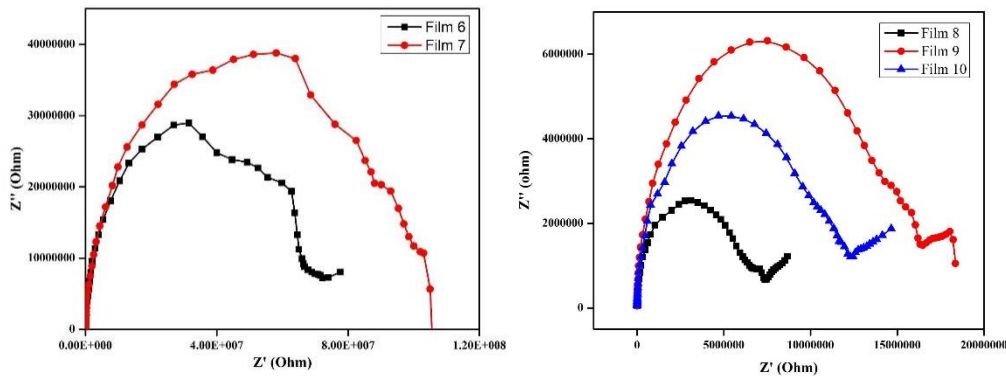


Figure 5. Impedance study of film 6 to 10.

Unexpectedly, film 8 exhibited a remarkable drop in resistance to $7.5 \times 10^6 \Omega$, signifying a substantial enhancement in conductivity compared to its predecessors. This striking decrease in resistance can be attributed to the optimal dispersion and alignment of MWCNTs within the PVA matrix, resulting in an improved percolation network for electron transport. However, films 9 and 10 displayed an abrupt increase in resistance, with values of $1.2 \times 10^7 \Omega$ and $1.6 \times 10^7 \Omega$, respectively, indicating a reduction in conductivity. This phenomenon may be attributed to an overloading of MWCNTs in the PVA matrix, leading to aggregation and disrupting the conductive pathways. The exceptional conductivity observed in film 8, with a value of $1.5 \times 10^8 \Omega^{-1}$ comparable to semiconductor materials, makes it an optimal candidate for further optoelectronic studies. The well-dispersed and interconnected MWCNTs in film 8 create an efficient electron transport network, highlighting its suitability for various optoelectronic applications. Interestingly, the diameter of the semicircle within the plot is observed to decrease with increasing temperature, eventually disappearing entirely at high temperatures.

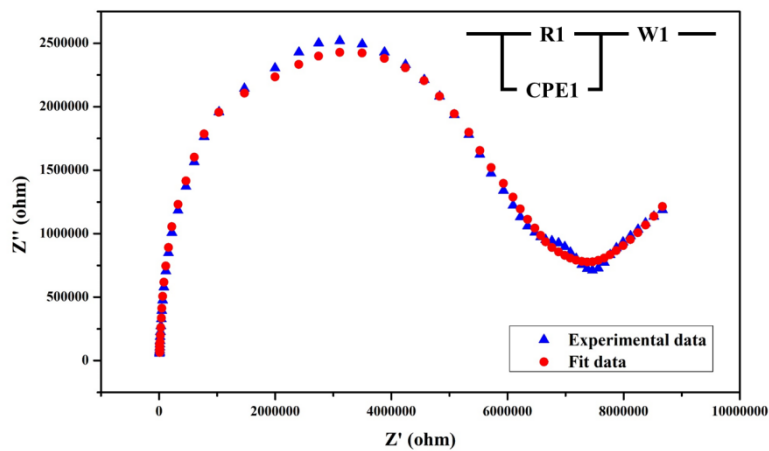


Figure 6. Experimental and fit data of impedance spectroscopy.

This shrinking diameter signifies a corresponding decrease in the bulk resistance of the material as temperature rises. This investigation underscores the critical role of MWCNT concentration in achieving the desired electrical properties in composite films, with an

optimum concentration striking the balance between dispersion and aggregation for enhanced conductivity. The complex impedance spectra point towards an equivalent circuit (Figure 6) representing the system's internal processes.

This circuit comprises a parallel combination of resistance (R1), reflecting the inherent opposition to current flow, and a constant phase element (CPE1) capturing non-ideal capacitive behavior in the polymer (represented by parameter "n"). In series with this combination is a Warburg element (W1) signifying the influence of diffusion-limited processes, potentially arising from pore size limitations. The high-frequency semicircle originates from the interaction between R1 and CPE1, revealing bulk polymer properties like conductivity and non-idealities. Conversely, the low-frequency spike attributed to W1 suggests that diffusion, potentially hindered by electrode surface roughness, plays a significant role at lower frequencies, offering valuable insights into the system's underlying physical mechanisms. The impedance of the CPE is represented as:

$$Z_{CPE} = A(j\omega)^{-n} \tag{2}$$

Where A is the inverse of capacitance and $\alpha = (1 - n)\frac{\pi}{2}$ where n is expressed in terms of α (the deviation from vertical spike in the Nyquist plot). For pure capacitance, the value of n = 1, and the lower value of n reflects the roughness of the electrode. The fitted results show that the assumed equivalent circuit fits the experimental data well.

Dielectric analysis better explains ion transport phenomena in polymer electrolyte systems. The real part of dielectric permittivity (ϵ') is proportional to the capacitance and measures the alignment of dipoles, whereas the imaginary part of dielectric permittivity (ϵ'') is proportional to conductance and represents the energy required to align the dipoles. The real and imaginary part of dielectric permittivity is evaluated using the impedance data:

$$\epsilon' = \frac{Z'}{\omega C_o(Z'^2 + Z''^2)} \tag{3}$$

$$\epsilon'' = \frac{Z''}{\omega C_o(Z'^2 + Z''^2)} \tag{4}$$

The dielectric relaxation process in polymer systems can be described by dielectric loss tangent ($\tan\delta$) [36]. It provides information about the energy lost or dissipated per cycle to the energy stored. $\tan\delta = \frac{\epsilon''}{\epsilon'}$

Figure 7 shows the plot of tangent loss as a function of frequency for a nanocomposite polymer system with varying Reline-MWCNT to polymer mass ratio. It is seen that the loss tangent increases with an increase in frequency, reaches maximum, and then finally decreases. The maxima or the peak value at a certain characteristic frequency shows the presence of relaxing dipoles [37]. The maximum in the dielectric loss peak is given by the relation:

$$\tau = \frac{1}{2\pi f_{max}} \tag{5}$$

Where τ is the estimated relaxation time for charge carriers [36], it is observed that for the 8th polymeric films, the f_{max} shifts towards the higher frequency side, which indicates that the relaxation phenomenon is thermally activated.

The relaxation frequency(ω) is found to be 5.4282 from the graph. Using relaxation frequency, the relaxation time is calculated with the formula $\omega\tau = 1$. The relaxation time(τ) is 0.18422 S.

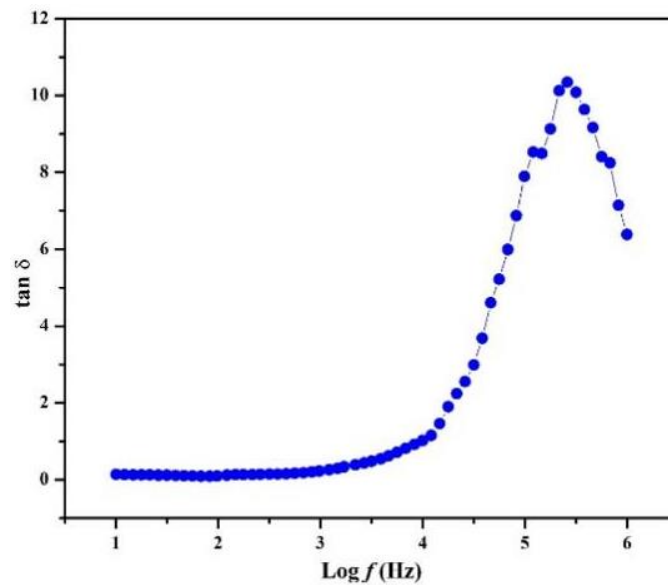


Figure 7. The dielectric loss tangent of film 8.

3.6. Refractive index.

Investigating the optical properties of film 8, particularly its refractive index (n), is essential for evaluating its suitability in specialized optoelectronic device fabrication. Figure 8 depicts the variation in n across refractive index as a function of wavelength. This variation can be quantitatively assessed using the formula provided in equation 2, where T_s represents the percentage transmittance.

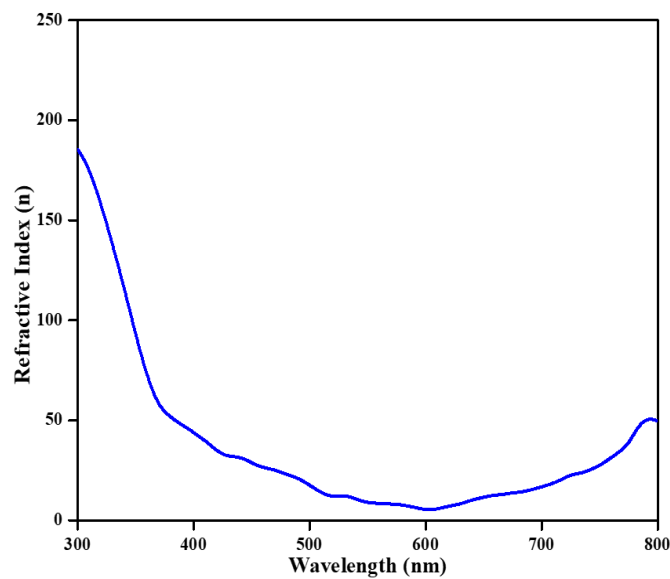


Figure 8. Refractive index (n) of film 8.

$$n = \frac{1}{T_s} + \sqrt{\frac{1}{T_s - 1}} \quad (6)$$

The refractive index study of the composite polymeric film 8 elucidated the various aspects of the material, such as optical scattering, absorption, and interference effects. In the 300-400 nm range, the refractive index decreases rapidly due to the strong light scattering properties of MWCNTs and potential absorption, along with nanotube-polymer interface effects. A remarkable refractive index minimum at around 600 nm suggests specific resonance or interference phenomena. Beyond this point, a gradual refractive index increase aligns with normal dispersion behavior in materials as longer wavelengths correspond to higher refractive

indices. These behaviors highlight the intricate interplay between the film's nanoscale structure, electronic properties, and incident light. The Reline-grafted MWCNTs, known for their electrical conductivity and high surface area, combined with the optically transparent PVA matrix, make the film a promising candidate for semiconducting optoelectronic applications such as photovoltaics and sensors, where precise refractive index control is essential for optimizing device performance. This section may be divided by subheadings. It should provide a concise and precise description of the experimental results, their interpretation, and the conclusions that can be drawn.

4. Conclusions

In summary, this study has unveiled a ground-breaking advancement in the realm of optoelectronic materials by integrating Reline grafted MWCNTs within the PVA matrix. The resulting composite films exhibit a unique blend of properties, making them highly promising for various optoelectronic applications. Characterization efforts have elucidated the films' structural, optical, electrical, and morphological attributes, highlighting their exceptional potential. Notably, the reduction in band gap energy with increasing MWCNT concentration from 5.8 eV of pure PVA to 1.8 eV and the remarkable enhancement in electrical conductivity in film 8 signifies the films' suitability for various optoelectronic devices. This reduction can be attributed to the combined effect of the dimensions of MWCNTs and the interaction with Reline molecules, which confine the movement of electrons. MWCNTs, with their inherent high conductivity, create a network for efficient charge transfer within the PVA matrix. Reline, acting as an electron acceptor, facilitates the transfer of electrons from the valence band of PVA to the conduction band of MWCNTs. This intermolecular charge transfer effectively narrows the bandgap, paving the way for the film's promising applications in optoelectronic devices with efficient light absorption and charge mobility. Moreover, refractive index studies underscore the film's potential for semiconducting optoelectronic applications. These findings pave the way for innovative applications in photonics, electronics, and beyond as researchers continue exploring the diverse possibilities of this unique composite material. In essence, the integration of Reline-MWCNTs within a PVA matrix represents a significant leap forward in the development of tailored optoelectronic materials, with the potential to revolutionize transparent conductive layers, photovoltaic materials, sensors, and various other optoelectronic device applications, driving advancements in the fields of materials science and technology.

Funding

This research received no external funding.

Acknowledgments

We acknowledge CHRIST University for its encouragement and support.

Conflicts of Interest

The authors declare no conflict of interest.

References

1. Lucherelli, M.A.; Duval, A.; Avérous, L. Biobased vitrimers: Towards sustainable and adaptable performing

- polymer materials. *Prog. Polym. Sci.* **2022**, *127*, 101515, <https://doi.org/10.1016/j.progpolymsci.2022.101515>.
2. Albertsson, A.-C.; Karlsson, S. Environment-adaptable polymers. *Polym. Degrad. Stab.* **1993**, *41*, 345-349, [https://doi.org/10.1016/0141-3910\(93\)90082-T](https://doi.org/10.1016/0141-3910(93)90082-T).
 3. Dalton, L.; Harper, A.; Ren, A.; Wang, F.; Todorova, G.; Chen, J.; Zhang, C.; Lee, M. Polymeric Electro-optic Modulators: From Chromophore Design to Integration with Semiconductor Very Large Scale Integration Electronics and Silica Fiber Optics. *Ind. Eng. Chem. Res.* **1999**, *38*, 8-33, <https://doi.org/10.1021/ie9705970>.
 4. Khonina, S.N.; Voronkov, G.S.; Grakhova, E.P.; Kazanskiy, N.L.; Kutluyarov, R.V.; Butt, M.A. Polymer Waveguide-Based Optical Sensors—Interest in Bio, Gas, Temperature, and Mechanical Sensing Applications. *Coatings* **2023**, *13*, 549, <https://doi.org/10.3390/coatings13030549>.
 5. Ta, V.D.; Wang, Y.; Sun, H. Microlasers Enabled by Soft-Matter Technology. *Adv. Opt. Mater.* **2019**, *7*, 1900057, <https://doi.org/10.1002/adom.201900057>.
 6. Nespola, A.; Abrate, S.; Gaudino, R.; Zerna, C.; Offenbeck, B.; Weber, N. High-Speed Communications Over Polymer Optical Fibers for In-Building Cabling and Home Networking. *IEEE Photonics J.* **2010**, *2*, 347-358, <https://doi.org/10.1109/JPHOT.2010.2048202>.
 7. Abbott, A.P.; Capper, G.; Davies, D.L.; Rasheed, R.K.; Tambyrajah, V. Novel solvent properties of choline chloride/urea mixtures. *Chem. Commun.* **2003**, 70-71, <https://doi.org/10.1039/b210714g>.
 8. Soni, S.K.; Thomas, B.; Kar, V.R. A Comprehensive Review on CNTs and CNT-Reinforced Composites: Syntheses, Characteristics and Applications. *Mater. Today Commun.* **2020**, *25*, 101546, <https://doi.org/10.1016/j.mtcomm.2020.101546>.
 9. Aslam, M.; Kalyar, M.A.; Raza, Z.A. Polyvinyl alcohol: A review of research status and use of polyvinyl alcohol based nanocomposites. *Polym. Eng. Sci.* **2018**, *58*, 2119-2132, <https://doi.org/10.1002/pen.24855>.
 10. Kataria, S.; Mudila, H.; Kumar, A.; Prasher, P. Optical properties of novel materials for optoelectronic applications. *Nanosci. Nanotechnol. - Asia* **2022**, *12*, 48-57, <https://doi.org/10.2174/2210681213666221031103157>.
 11. Wang, G.; Liu, T.; Chao, J.; Jin, H.; Liu, J.; Zhang, H.; Lyu, W.; Yin, P.; Al-Ghamdi, A.; Wageh, S.; Fu, B.; Zhang, H. Recent Advances and Challenges in Ultrafast Photonics Enabled by Metal Nanomaterials. *Adv. Optical Mater.* **2022**, *10*, 2200443, <https://doi.org/10.1002/adom.202200443>.
 12. Nasibi S, Nargesi khoramabadi H, Arefian M, et al A review of Polyvinyl alcohol / Carboxiy methyl cellulose (Nargesi khoramabadi, H.; Arefian, M.; Hojjati, M.; Tajzad, I.; Mokhtarzade, A.; Mazhar, M.; Jamavari, A. A review of Polyvinyl alcohol / Carboxymethyl cellulose (PVA/CMC) composites for various applications. *J. Compos. Compd.* **2020**, *2*, 69-76, <https://doi.org/10.29252/jcc.2.2.2>.
 13. Lomba, L.; Ribate, M.P.; Sangüesa, E.; Concha, J.; Garralaga, M. P.; Errazquin, D.; García, C.B.; Giner, B. Deep Eutectic Solvents: Are They Safe? *Appl. Sci.* **2021**, *11*, 10061, <https://doi.org/10.3390/app112110061>.
 14. Kist, J.A.; Zhao, H.; Mitchell-Koch, K.R.; Baker, G.A. The study and application of biomolecules in deep eutectic solvents. *J. Mater. Chem. B* **2021**, *9*, 536-566, <https://doi.org/10.1039/d0tb01656j>.
 15. El Achkar, T.; Greige-Gerges, H.; Fourmentin, S. Basics and properties of deep eutectic solvents: a review. *Environ. Chem. Lett.* **2021**, *19*, 3397-3408, <https://doi.org/10.1007/s10311-021-01225-8>.
 16. Kareem, A.A.; Rasheed, H.K. Electrical and thermal characteristics of MWCNTs modified carbon fiber/epoxy composite films. *Mater. Sci.-Pol.* **2019**, *37*, 622–627, <https://doi.org/10.2478/msp-2019-0081>.
 17. Qu, J.; Tian, M.; Han, X.; Zhang, R.; Wang, Q. Photo-thermal conversion characteristics of MWCNT-H₂O nanofluids for direct solar thermal energy absorption applications. *Appl. Therm. Eng.* **2017**, *124*, 486-493, <https://doi.org/10.1016/j.applthermaleng.2017.06.063>.
 18. Svigelj, R.; Dossi, N.; Grazioli, C.; Toniolo, R. Deep Eutectic Solvents (DESs) and Their Application in Biosensor Development. *Sensors* **2021**, *21*, 4263, <https://doi.org/10.3390/s21134263>.
 19. Khan, S.A.; Zain, Z.M.; Mansoor, M.; Mahfuz, M.M.H.; Rahman, A.; Rashid, M.A.N.; Rais, M.S. Performance investigation of ZnO/PVA nanocomposite film for organic solar cell. *Mater. Today Proc.* **2021**, *47*, 2615-2621, <https://doi.org/10.1016/j.matpr.2021.05.197>.
 20. da Silva, W.; Ghica, M.E.; Brett, C.M.A. Biotoxic trace metal ion detection by enzymatic inhibition of a glucose biosensor based on a poly(brilliant green)–deep eutectic solvent/carbon nanotube modified electrode. *Talanta* **2020**, *208*, 120427, <https://doi.org/10.1016/j.talanta.2019.120427>.
 21. Özkan, Ş.; Çoban, Ö. The hybrid effects of basalt and PVA fiber on properties of a cementitious composite: Physical properties and non-destructive tests. *Constr. Build. Mater.* **2021**, *312*, 125292, <https://doi.org/10.1016/j.conbuildmat.2021.125292>.

22. Talianov, P.; Fatkhutdinova, L.I.; Timin, A.S.; Milichko, V.A.; Zyuzin, M.V. Adaptive Nanoparticle-Polymer Complexes as Optical Elements: Design and Application in Nanophotonics and Nanomedicine. *Laser Photonics Rev.* **2021**, *15*, 2000421, <https://doi.org/10.1002/lpor.202000421>.
23. Azhar, O.; Jahan, Z.; Sher, F.; Niazi, M.B.K.; Kakar, S.J.; Shahid, M. Cellulose acetate-polyvinyl alcohol blend hemodialysis membranes integrated with dialysis performance and high biocompatibility. *Mater. Sci. Eng. C* **2021**, *126*, 112127, <https://doi.org/10.1016/j.msec.2021.112127>.
24. Alrowaili, Z.A.; Taha, T.A.; El-Nasser, K.S.; Donya, H. Significant Enhanced Optical Parameters of PVA-Y₂O₃ Polymer Nanocomposite Films. *J. Inorg. Organomet. Polym.* **2021**, *31*, 3101-3110, <https://doi.org/10.1007/s10904-021-01995-2>.
25. Kavaya, H.V.; Nithin, K.S.; Kendagannaswamy, B.K.; Sachhidananda, S.; Chamaraja, N.A. Optical performance appraisal of mechanically flexible and visibly clear PVP-PVA/calcium doped zirconium oxide nanocomposites for UV shielding applications. *Optik* **2021**, *227*, 166008, <https://doi.org/10.1016/j.ijleo.2020.166008>.
26. Karadaş, S.; Yerişkin, S.A.; Balbaş, M.; Azizian-Kalandaragh, Y. Complex dielectric, complex electric modulus, and electrical conductivity in Al/(Graphene-PVA)/p-Si (metal-polymer-semiconductor) structures. *J. Phys. Chem. Solids* **2021**, *148*, 109740, <https://doi.org/10.1016/j.jpcs.2020.109740>.
27. Bulinski, M. Metal Doped PVA Films for Opto-Electronics-Optical and Electronic Properties, an Overview. *Molecules* **2021**, *26*, 2886, <https://doi.org/10.3390/molecules26102886>.
28. Hussain, S.; Iqbal, M.; Khan, A.A.; Khan, M.N.; Mehboob, G.; Ajmal, S.; Ashfaq, J.M.; Mehboob, G.; Ahmed, M.S.; Khisro, S.N.; Li, C.-J.; Chikwenze, R.; Ezugwu, S. Fabrication of Nanostructured Cadmium Selenide Thin Films for Optoelectronics Applications. *Front. Chem.* **2021**, *9*, 661723, <https://doi.org/10.3389/fchem.2021.661723>.
29. Zhang, C.; Ji, C.; Park, Y.-B.; Guo, L.J. Thin-Metal-Film-Based Transparent Conductors: Material Preparation, Optical Design, and Device Applications. *Adv. Opt. Mater.* **2021**, *9*, 2001298, <https://doi.org/10.1002/adom.202001298>.
30. Socol, M.; Preda, N. Hybrid Nanocomposite Thin Films for Photovoltaic Applications: A Review. *Nanomaterials* **2021**, *11*, 1117, <https://doi.org/10.3390/nano11051117>.
31. Yang, M.-R.; Chen, K.S. Humidity sensors using polyvinyl alcohol mixed with electrolytes. *Sens. Actuators B: Chem.* **1998**, *49*, 240–247, [https://doi.org/10.1016/s0925-4005\(98\)00134-8](https://doi.org/10.1016/s0925-4005(98)00134-8).
32. Dulmaa, A.; Cougnon, F.G.; Dedoncker, R.; Depla, D. On the grain size-thickness correlation for thin films. *Acta Mater.* **2021**, *212*, 116896, <https://doi.org/10.1016/j.actamat.2021.116896>.
33. Lu, M.; Meng, X.; Huang, R.; Chen, L.; Peyton, A.; Yin, W.; Qu, Z. Thickness measurement of circular metallic film using single-frequency eddy current sensor. *NDT & E Int.* **2021**, *119*, 102420, <https://doi.org/10.1016/j.ndteint.2021.102420>.
34. Shi, B.; Jia, J.; Feng, X.; Ma, G.; Wu, Y.; Cao, B. Thermal evaporated CuI film thickness-dependent performance of perovskite solar cells. *Vacuum* **2021**, *187*, 110076, <https://doi.org/10.1016/j.vacuum.2021.110076>.
35. Cullen, C.P.; Ó Coileáin, C.; McManus, J.B.; Hartwig, O.; McCloskey, D.; Duesberg, G.S.; McEvoy, N. Synthesis and characterisation of thin-film platinum disulfide and platinum sulfide. *Nanoscale* **2021**, *13*, 7403-7411, <https://doi.org/10.1039/d0nr06197b>.
36. Li, B.; Matsutani, H.; Kimura, M.; Miyatake, M.; Murakami, Y.; Katoh, S.; Tanimoto, A.; Ma, X.; Jiang, X. Application of decarboxylation reactions for improvement of dielectric properties of a methacrylic polymer. *RSC Adv.* **2021**, *11*, 20926-20932, <https://doi.org/10.1039/d1ra01626a>.
37. Aziz, S.B.; Nofal, M.M.; Abdulwahid, R.T.; O. Ghareeb, H.; Dannoun, E.M.A.; M. Abdullah, R.; Hamsan, M.H.; Kadir, M.F.Z. Plasticized Sodium-Ion Conducting PVA Based Polymer Electrolyte for Electrochemical Energy Storage—EEC Modeling, Transport Properties, and Charge-Discharge Characteristics. *Polymers* **2021**, *13*, 803, <https://doi.org/10.3390/polym13050803>.